We are IntechOpen,
the world's leading publisher of
Open Access books
Built by scientists, for scientists

4,800
Open access books available

122,000
International authors and editors

135M
Downloads

Our authors are among the

154
Countries delivered to

TOP 1%
most cited scientists

12.2%
Contributors from top 500 universities

BOOK CITATION INDEX
CLARIVATE ANALYTICS
INDEXED

WEB OF SCIENCE™

Selection of our books indexed in the Book Citation Index
in Web of Science™ Core Collection (BKCI)

Interested in publishing with us?
Contact book.department@intechopen.com

Numbers displayed above are based on latest data collected.
For more information visit www.intechopen.com

Computational Study of Thermal, Water and Gas Management in PEM Fuel Cell Stacks

Agus P. Sasmito, Erik Birgersson and Arun S. Mujumdar

Additional information is available at the end of the chapter

1. Introduction

The overall high degree of research and development of PEM fuel cells over the last few decades has led to a series of improvements. Noteworthy is the `jump' in cell performance that was achieved from 50-100 W m^{-2} in 1959-1961 with a phenol sulfonic membrane to 6000-8000 W m^{-2} in 1971-1980 by the introduction of the Nafion membrane (Costamagna, 2001). Around thirteen years later, the first fuel cell was brought from laboratory to power a car in the New Generation of Vehicle program (PNGV) in the US in 1993 (Costamagna, 2001b); moreover, in 2007, the vehicle manufacturer Honda launched a fuel cell car FCX clarity and commercially available in 2008. The PEM fuel cells have recently passed the demonstration phase and have partially reached the commercialization stage because of the rapid development and impressive research effort worldwide. However, despite the promising achievements and plausible prospects for PEM fuel cell, in view of the remaining challenges, it is commonly agreed that there is still a long way to go before they can successfully and economically replace the various traditional energy systems (Hellman et al., 2007).

Currently, there are three major challenges in fuel cell research and development which need to be improved (Martin et al., 2010 and Steiner et al., 2009):

- *Cost*: The current cost of a PEFC for automotive application is approximately 600-1000 $/kW (Tsuchiya and Kobayashi, 2004, Mock and Schmid, 2009) which means that the cost of a vehicle powered by fuel cell is about 10 times than that of the traditional car with an internal combustion engine; the total cost of a PEM fuel cell for stationary applications and combined heat power system is around 23000 Euro per kW (Staffell and Green, 2009). In order to be able to compete with traditional power sources, the US Department of Energy (DOE) has set targets for hydrogen and fuel cell technologies. The targets for automotive fuel cells cost is around 30 $/kW by 2015; whereas, for stationary application, the targets is at fuel cell cost of 750 $/kW (Martin et al., 2010).

- *Durability*: For a fuel cell operating under constant load conditions, e.g., in stationary applications, the degradation rate can be as low as 1-10 μV/h (Wolfgang et al., 2008), this would result in 40-80 mV performance loss over 40000 h, i.e. an efficiency and power loss of 10% over 40000 h lifetime (Brujin et al., 2007). However, the degradation rates can increase by orders of magnitude when conditions include load cycling, start-stop cycles, low humidification or humidification cycling, temperatures of 90 °C or higher and fuel starvation. Such conditions are expected for automotive applications. Currently, the typical durability for fuel cell in automotive application is less than 5000 h (equivalent to 150000 miles); for example, Mercedes-Benz claims a lifetime of above 2000 h without performance degradation for their current fuel cell stacks operated in test-vehicles. Hence, US DOE has also set targets for fuel cell durability to be improved up to 5000 and 40000 h for automotive and stationary applications, respectively, by 2015 (Martin et al., 2010).

- *Performance*: Fuel cell performance has improved rapidly in recent years; the performance improved from 300 W m^{-2} in the NASA Gemini project in 1960 to power densities of about 6000 Wm^{-2} for more recent fuel cell stack, e.g., Ballard MK 900 (Mock and Schmid, 2009). Although power densities of 10000 Wm^{-2} and even higher have already been met in the laboratory, there is still an interdependencies between fuel cell performance and catalyst loading. Hence, US DOE has set a target for power densities of 10000 W m^{-2} with fuel cell efficiency 60 % by 2015 (Martin et al., 2010 and Mock and Schmid, 2009).

Out of all these challenges, this chapter will mainly focus on the performance improvement as fuel cell can be considered as immature and complex technology. Immaturity is reflected by the rapid technological progress in performance, e.g. power density, capacity, sustainability and cost (Hellman et al., 2007). Whereas, complexity refers to the fact that fuel cells require an overall system that comprises of numerous components between which there is a high degree of interdependence. Furthermore, these two issues are correlated with PEM fuel cell performance improvement and cost reduction (Sopian et al., 2006). To achieve these goals, a significant effort on research and development in the worldwide fuel cell area focuses on high-purity hydrogen, cost reduction of the system, including fuel cell material, where the cost of the bipolar plate and the electrode including platinum make up approximately 80% of the total cost of PEM fuel cell (Mock and Schmid, 2009, Tsuchiya and Kobayashi, 2004, Hermann et al., 2005), and various technological problems (Wee et al., 2007).

In order to improve fuel cell system performance, one needs to address three issues that are most vital to the PEM fuel cell performance (Sasmito et al., 2011):

- *Thermal management*: An effective heat removal system is necessary to keep the fuel cell/stack at a uniform operating temperature, as a significant amount of heat is generated in a fuel cell. As it is known that fuel cells are usually about 30-60% electrically efficient at typical operating power density; hence, energy which is not converted into electrical power is dissipated as heat. For a stack, to achieve high stack

performance, each and every cell should be running at identical operating conditions. Hence, either an active or a passive cooling system should be applied (Sasmito, et al., 2011a). Active cooling usually either involves coolant channels in the bipolar plate or as separate layers, where coolant liquid is pumped through to remove heat, or external fans to improve the air flow through the fuel cell/stack. For passive cooling, natural convection can be employed to remove heat. However, this mode of cooling is only sufficient for small portable fuel cells with power rating of less than 100 W (Sasmito et al., 2010 and Sasmito 2011b). Another option for passive cooling is edge-cooling, which means that if the fuel cell is made narrow enough, the heat generated may be removed on the sides of the cell by attaching fins and/or selecting high thermal conductivity material (Sasmito et al., 2011).

- *Water management*: Since the PEM fuel cell operates at temperatures below 100 °C, water vapor can condense and form a liquid phase inside the fuel cell (Sasmito et al., 2011c). Hence, to prevent flooding of the various cell components while keeping the membrane sufficiently hydrated for ionic conduction, a proper water management should be applied together with thermal management. Several techniques have been employed in order to mitigate water flooding in cathode PEFC such as proper flow field design, anode water removal, operating condition control and so forth. More advanced techniques can be employed, e.g. hydrophobic bipolar plates together with electro-osmotic pumps (Buie et al., 2006). This setup can be used to pump water into the cell if it is too dry or to pump out water if the cell is flooding. Furthermore, a frequent automatic purge can also be implemented to avoid liquid flooding in a dead-end anode PEM fuel cell (Sasmito et al., 2011d).

- *Gas management*: To ensure that enough hydrogen and oxygen reach the active layer to generate current, especially so at high current densities. In addition, uniformly distributed fuel and reactant is a requirement to generate uniform current distribution and thus utilize the catalyst evenly (Sasmito et al., 2011e).

The main objective of this chapter is to address fuel cell issues related to various technological problems, which could improve the fuel cell system performance by optimal thermal, gas, and water management. This research is concerned with the fundamental issues as well as application of PEM fuel cells:

- *Fundamental research*: The fundamental aspects concern the transport phenomena that can be found in a PEM fuel cell: phenomena that are inherently multiscale (time and space) in nature, including heat and mass transfer, electrochemistry, two-phase flow, charge transfer, agglomerate catalyst layers, and transport in the membrane. Here, a one-domain, two-phase-flow model comprising conservation of equations of mass, momentum, species, energy, charge, an agglomerate catalyst layer and a phenomenological membrane model is developed, calibrated and further validated with experimental polarization curves, iR-corrected curves, and local current density distributions. After validation, to ensure the fidelity of model predictions, the model is extended to account for a fuel cell stack together with its surrounding environment and auxiliary equipment, such as fans; thus, allowing for studies that not only capture the

essential physics of the fuel cell stack but also the interaction with auxiliary equipment. Furthermore, the model is also extended to account for transient characteristics of PEM fuel cell operating with a dead-end anode

- *Applied research*: The applied aspects address key issues related to thermal, water, and gas management, as well as design and optimization to ensure optimal or near-to optimal fuel cell performance. Four different thermal management strategies – liquid-cooling, forced air-convection cooling, edge-air cooling, and natural-convection cooling – as well as various designs and conditions commonly employed in PEM fuel cell stacks are investigated. Furthermore, a new concept to enhance thermal management in PEFC stack is proposed. In addition, we also address gas and water management issues in a PEM fuel cell with a dead-end anode.
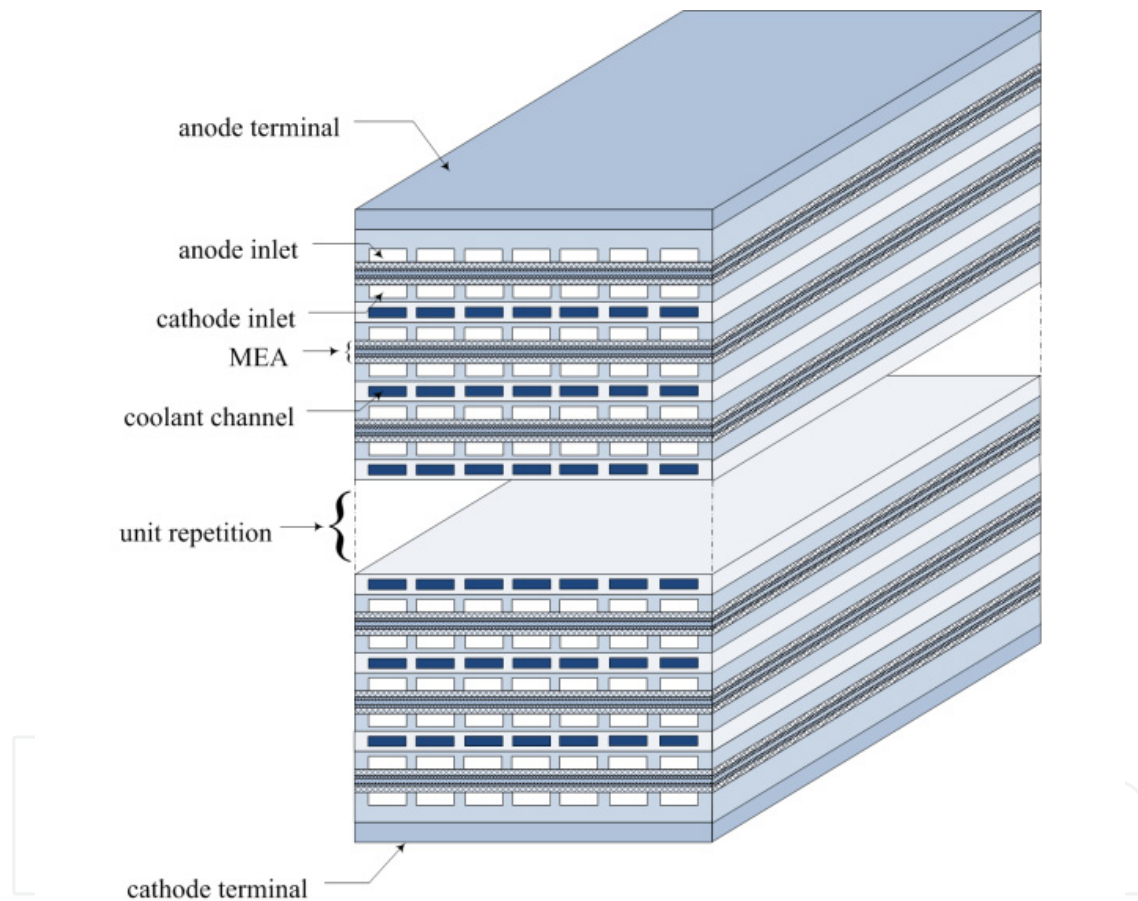

Figure 1. Schematic of PEM fuel cell stack

2. Model formulation

Several coupled transient transport phenomena take place within the PEFC which comprises of two sets of flow channels, anode and cathode gas diffusion layers, anode and cathode catalyst layers and a polymer electrolyte membrane, see Fig. 1 for details. They include:

- Convective heat and mass transfer in the flow channels;

- Diffusion in the gas diffusion layers;
- Two-phase flow/transport in the gas diffusion layers and flow fields (water in vapor and liquid phases);
- Phase change in the gas diffusion layers and flow channels;
- Electrochemical reactions in the catalyst layers;
- Heat generation in the catalyst layers;
- Water production in the cathode catalyst layer;
- Oxygen consumption in the cathode catalyst layer;
- Hydrogen consumption in the anode catalyst layer;
- Electron transport in the gas diffusion layers and bipolar plates;
- Membrane water transport;
- Proton transport in the membrane;
- Electro-osmotic drag in the membrane;
- Diffusion of H_2/O_2/N_2 through the membrane;
- Ohmic heating in the membrane, catalyst layers, gas diffusion layers, and bipolar plates;
- Conjugate heat transfer between bipolar plates/cooling channels and bipolar plates/flow channels.

Starting from the basic physics equation and governing equation, electrochemical reactions, two-phase flow and its constitutive relations to a numerical model are summarized. The model accounts for the following transport phenomena in each cell for the stack:

- *Mass, momentum and species transfer*: Conservation of two-phase mass, momentum and species is considered in the whole cell, with certain simplifications for the membrane. The gas phase consists of hydrogen, oxygen, water vapour and nitrogen, whereas the liquid phase is assumed to comprise only of liquid water due to the low solubility of the other gases.
- *Heat transfer*: We consider convection, conduction, evaporation/condensation, ohmic heating, entropy generation and heat generation due to the activation overpotential.
- *Charge transfer*: Conservation of charge and Ohm's law is solved.

The main model assumptions/approximations are:

- *Thermal equilibrium*: We assume local thermal equilibrium between all phases.
- *Membrane*: The membrane model takes into account the flux of water due to electroosmotic drag and diffusion. In this work, a GORE membrane is employed for which we modify the standard phenomenological equations derived for a Nafion® with a correction factor.
- *Two-phase flow*: We assume that the dominating driving force for liquid transport inside the gas diffusion layers and catalyst layers is capillarity. In the flow fields, we consider a mist flow approximation of the liquid flow, for which the liquid velocity is assumed to be the same as the gas velocity, as well as the capillary contribution due the porous nature of the net-type flow fields we solve for here.
- *Catalyst layers*: An agglomerate model is implemented to account for mass transfer inside the cathode catalyst layer. Here, we assume the agglomerate nucleus to be

spherical in shape, which in turn is covered by a thin film of ionomer and water (Sasmito et al., 2011). For the anode, a conventional expression based on the Butler-Volmer equation is employed as the overpotential is significantly lower than at the cathode.

- *End-plates*: We assume that the stack comprises a large number of cells, so that the effects of the two end plates are negligible for the overall stack performance.

The governing equations together with the constitutive relations and appropriate boundary conditions are then solved numerically.

In this chapter, the superscripts (g), (l) and (m) denote properties associated with the gas, liquid, solid and membrane, respectively, and (c) denotes any quantity associated with capillary pressure

2.1. Fuel cell stack

We consider conservation of mass, momentum, species, energy, charge, phenomenological membrane model and two-phase in the separator plates, flow fields, gas diffusion layers, catalyst layers, and membrane in the PEMFC, expressed as

$$\nabla \cdot \left(\rho^{(g)} \mathbf{u}^{(g)} \right) = S_{mass} - \dot{m}_{H_2O} \tag{1}$$

$$\nabla \cdot \left(\rho^{(l)} \mathbf{u}^{(l)} \right) = \dot{m}_{H_2O} \tag{2}$$

$$\nabla \cdot \left(\rho^{(g)} \mathbf{u}^{(g)} \mathbf{u}^{(g)} \right) = \nabla \cdot \boldsymbol{\sigma} - \frac{\mu^{(g)}}{\kappa} \mathbf{u}^{(g)} \tag{3}$$

$$\nabla \cdot \left(\rho^{(g)} C_p^{(g)} \mathbf{u}^{(g)} T \right) = \nabla \cdot \left(k_{eff} \nabla T \right) + S_{temp} \tag{4}$$

$$\nabla \cdot \mathbf{n}_i^{(g)} = S_i \tag{5}$$

$$\nabla \cdot \mathbf{n}_{H_2O}^{(m)} = 0 \tag{6}$$

$$\nabla \cdot \mathbf{i}^{(m)} = S_{pot} \tag{7}$$

$$\nabla \cdot \mathbf{i}^{(s)} = -S_{pot} \tag{8}$$

In the above equations, $\rho^{(g,l)}$ denote phase densities, $\mathbf{u}^{(g,l)} = \left(u^{(g,l)}, v^{(g,l)} \right)$ are the phase velocities (in x and y directions), $\dot{m}_{H_2O}$ is the interphase mass transfer of water between the gas and liquid phase, $\boldsymbol{\sigma}$ is the total stress tensor, $\mu^{(g)}$ is the gas dynamic viscosity, κ is the permeability, $c_p^{(g)}$ is the specific heat capacity, T is the temperature and k_{eff} is the effective thermal conductivity. Furthermore, $\mathbf{i}^{(m)}$ and $\mathbf{i}^{(s)}$ are the current densities carried by protons

and electrons respectively. The governing equations are similar to those implemented by Li et al.(2004) and Schwarz and and Djilali (2007).

The total stress tensor, mass fluxes of species, current densities and liquid water velocity are defined as

$$\boldsymbol{\sigma} = -p^{(g)}\mathbf{I} + \mu^{(g)}\left(\nabla\mathbf{u}^{(g)} + \left(\nabla\mathbf{u}^{(g)}\right)^{\mathbf{T}}\right) - \frac{2}{3}\mu^{(g)}\left(\nabla\cdot\mathbf{u}^{(g)}\right)\mathbf{I} \tag{9}$$

$$\mathbf{n}_i^{(g)} = \rho^{(g)}\mathbf{u}^{(g)}\omega_i^{(g)} - \rho^{(g)}D_{i,\text{eff}}^{(g)}\nabla\omega_i^{(g)} \quad (i = H_2, O_2, H_2O, N_2) \tag{10}$$

$$\mathbf{n}_{H_2O}^{(m)} = \frac{n_d M_{H_2O}}{F}\mathbf{i}^{(m)} - \frac{\rho^{(m)}}{M^{(m)}}M_{H_2O}D_{H_2O,\text{eff}}^{(m)}\nabla\lambda \tag{11}$$

$$\mathbf{i}^{(m)} = -\sigma_{\text{eff}}^{(m)}\nabla\phi^{(m)} \tag{12}$$

$$\mathbf{i}^{(s)} = -\sigma_{\text{eff}}^{(s)}\nabla\phi^{(s)} \tag{13}$$

$$\mathbf{u}^{(l)} = \begin{cases} \mathbf{u}^{(g)}s - D^{(c)}\nabla s & \text{(ff)} \\ -D^{(c)}\nabla s & \text{(gdl, cl)} \end{cases} \tag{14}$$

For the total stress tensor in Eq. 9, $p^{(g)}$ is the gas pressure and $\mathbf{I}$ is the identity matrix. Here, we solve for a species mixture of hydrogen (H_2), water (H_2O), oxygen (O_2) and nitrogen (N_2); $\omega_i^{(g)}$ denotes the mass fraction of species i in the gas phase, and $D_{i,\text{eff}}^{(g)}$ represents the effective diffusivity in the gas phase. The flux of water in the membrane, Eq. 11, is expressed with a phenomenological model in terms of the membrane water content, λ, which account for the electroosmotic drag (first term on the right hand side [RHS]) and diffusion (second term on the RHS). Here, n_d is the electroosmotic drag coefficient, F is Faraday's constant, $D_{H_2O,\text{eff}}^{(m)}$ is the effective diffusivity of water in the membrane, $\rho^{(m)}$ and $M^{(m)}$ are the density and equivalent weight of the dry membrane, respectively. In Eqs. 12 and 13, $\phi^{(m)}$ and $\phi^{(s)}$ represent the potential of the ionic phase and the solid phase, while $\sigma_{\text{eff}}^{(m)}$ and $\sigma_{\text{eff}}^{(s)}$ are the electrical conductivities of proton and electron transport, respectively. In Eq. 14, s is the liquid saturation and $D^{(c)}$ is the capillary diffusion.

The source terms in Eqs. 1-8 are given by

$$S_{\text{mass}} = \begin{cases} -\dfrac{M_{O_2}}{4F}J_c + \dfrac{M_{H_2O}}{2F}J_c - \nabla\cdot\mathbf{n}_{H_2O}^{(m)} & \text{(cathode cl)} \\ -\dfrac{M_{H_2}}{2F}J_a - \nabla\cdot\mathbf{n}_{H_2O}^{(m)} & \text{(anode cl)} \\ 0 & \text{(elsewhere)} \end{cases} \tag{15}$$

$$
S_i \begin{cases}
-\dfrac{M_{O_2}}{4F} J_c & (O_2,\ \text{cathode cl}) \\[2ex]
+\dfrac{M_{H_2O}}{2F} J_c - \nabla \cdot \mathbf{n}^{(m)}_{H_2O,eff} - \dot{m}_{H_2O} & (H_2O,\ \text{cathode cl}) \\[2ex]
-\nabla \cdot \mathbf{n}^{(m)}_{H_2O,eff} - \dot{m}_{H_2O} & (H_2O,\ \text{anode cl}) \\[2ex]
-\dot{m}_{H_2O} & (H_2O,\ \text{gdl}) \\[2ex]
-\dfrac{M_{H_2}}{2F} J_a & (H_2,\ \text{anode cl}) \\[2ex]
0 & (\text{elsewhere})
\end{cases}
\tag{16}
$$

$$
S_{pot} \begin{cases}
-J_c & (\text{cathode cl}) \\[1ex]
J_a & (\text{anode cl}) \\[1ex]
0 & (\text{elsewhere})
\end{cases}
\tag{17}
$$

$$
S_{temp} = \begin{cases}
J_c\left(-T\dfrac{\partial E_{rev}}{\partial T} + |\eta_c|\right) + \sigma^{(m)}_{eff}\left(\nabla \phi^{(m)}\right)^2 + \\
\qquad + \sigma^{(s)}_{eff}\left(\nabla \phi^{(s)}\right)^2 + \dot{m}_{H_2O} H_{vap} & (\text{cathode cl}) \\[2ex]
J_a \eta_a + \sigma^{(m)}_{eff}\left(\nabla \phi^{(m)}\right)^2 + \\
\qquad + \sigma^{(s)}_{eff}\left(\nabla \phi^{(s)}\right)^2 + \dot{m}_{H_2O} H_{vap} & (\text{anode cl}) \\[2ex]
\sigma^{(m)}_{eff}\left(\nabla \phi^{(m)}\right)^2 & (\text{m}) \\[2ex]
\sigma^{(s)}_{eff}\left(\nabla \phi^{(s)}\right)^2 + \dot{m}_{H_2O} H_{vap} & (\text{gdl}) \\[2ex]
\sigma^{(s)}_{eff}\left(\nabla \phi^{(s)}\right)^2 & (\text{ff, sp})
\end{cases}
\tag{18}
$$

The source term in Eq. 15 comprises mass consumption and production due to electrochemical reactions and the transport of water through the membrane, whilst the source terms for species conservation, Eq. 16, considers species consumption and production due to electrochemical reactions as well as interphase mass transfer for water and the transport of water through membrane. In catalyst layer, λ is defined by solving Eq. 75 and 76. In Eq. 17, $J_{a,c}$ ($J_{a,c} > 0$) denote the volumetric current densities, η_a ($\eta_a > 0$) and η_c ($\eta_c < 0$) are the overpotential at the anode and cathode, and E_{rev} is the reversible potential. Heat source from the reversible and irreversible entropic generated by the electrochemical reactions can be found in the first two terms of Eq. 18, the third and forth describe ohmic heating, while the energy transfer due to interphase mass transfer is described in the last term, where H_{vap} is the heat of vaporization of water.

2.2. Coolant plates

We solve for conservation of mass (incompressible liquid), momentum, energy, and charge in the coolant plates, given by

$$\nabla \cdot \left(\rho^{(l)} \mathbf{u}^{(l)} \right) = 0 \tag{19}$$

$$\nabla \cdot \left(\rho^{(l)} \mathbf{u}^{(l)} \mathbf{u}^{(l)} \right) = \nabla \cdot \boldsymbol{\sigma} - \frac{\mu^{(l)}}{\kappa} \mathbf{u}^{(l)} \tag{20}$$

$$\nabla \cdot \left(\rho^{(l)} C_{\mathrm{p}}^{(l)} \mathbf{u}^{(l)} T \right) = \nabla \cdot \left(k_{\mathrm{eff}} \nabla T \right) \tag{21}$$

$$\nabla \cdot \mathbf{i}^{(s)} = 0 \tag{22}$$

where the total stress tensor and current density are defined as

$$\boldsymbol{\sigma} = -p^{(l)} \mathbf{I} + \mu^{(l)} \left(\nabla \mathbf{u}^{(l)} + \left(\nabla \mathbf{u}^{(l)} \right)^{\mathbf{T}} \right) \tag{23}$$

$$\mathbf{i}^{(s)} = -\sigma_{\mathrm{eff}}^{(s)} \nabla \phi^{(s)} \tag{24}$$

3. Constitutive relations

The gas density (assuming ideal gas) is defined as

$$\rho^{(g)} = \frac{p^{(g)} M^{(g)}}{RT} \tag{25}$$

where

$$M^{(g)} = \left(\omega_{\mathrm{H}_2}^{(g)} / M_{\mathrm{H}_2} + \omega_{\mathrm{O}_2}^{(g)} / M_{\mathrm{O}_2} + \omega_{\mathrm{H}_2\mathrm{O}}^{(g)} / M_{\mathrm{H}_2\mathrm{O}} + \omega_{\mathrm{N}_2}^{(g)} / M_{\mathrm{N}_2} \right)^{-1} \tag{26}$$

The mass fraction of nitrogen is given by

$$\omega_{\mathrm{N}_2}^{(g)} = 1 - \omega_{\mathrm{H}_2}^{(g)} - \omega_{\mathrm{O}_2}^{(g)} - \omega_{\mathrm{H}_2\mathrm{O}}^{(g)} \tag{27}$$

The molar fractions are related to the mass fractions as

$$x_{\mathrm{i}}^{(g)} = \frac{\omega_{\mathrm{i}}^{(g)} M^{(g)}}{M_{\mathrm{i}}} \tag{28}$$

The molar concentrations are given by

$$c_{\mathrm{i}}^{(g)} = \frac{\omega_{\mathrm{i}}^{(g)} \rho^{(g)}}{M_{\mathrm{i}}} \tag{29}$$

The gas mixture viscosity, $\mu^{(g)}$, is defined as

$$\mu^{(g)} = \sum_\alpha \frac{x_\alpha^{(g)} \mu_\alpha^{(g)}}{\sum_\beta x_\alpha^{(g)} \Phi_{\alpha,\beta}} \qquad \text{with } \alpha, \beta = H_2, O_2, H_2O, N_2 \tag{30}$$

where $x_{\alpha,\beta}^{(g)}$ are the mole fraction of species α and β, and

$$\Phi_{\alpha,\beta} = \frac{1}{\sqrt{8}} \left(1 + \frac{M_\alpha}{M_\beta}\right)^{-1/2} \left[1 + \left(\frac{\mu_\alpha^{(g)}}{\mu_\beta^{(g)}}\right)^{\frac{1}{2}} \left(\frac{M_\beta}{M_\alpha}\right)^{\frac{1}{4}}\right]^2 \tag{31}$$

The effective thermal conductivity is defined as

$$k_{\text{eff}} = \varepsilon(1-s)\left(\sum k_i^{(g)} \omega_i^{(g)}\right) + \varepsilon s k_{H_2O}^{(l)} + (1-\varepsilon) k^{(s)} \tag{32}$$

where $k^{(l)}$ is the thermal conductivity of liquid water, ε is the porosity, and $k^{(s)} = \left(k_{co}^{(s)}, k_{sp}^{(s)}, k_{ff}^{(s)}, k_{gdl}^{(s)}, k_{cl}^{(s)}, k_m^{(s)}\right)$ are the thermal conductivities of the solid phases in various functional layers. The gas mixture specific heat capacity, $c_p^{(g)}$, is written as

$$c_p^{(g)} = \sum_i \omega_i^{(g)} c_{p,i}^{(g)} \tag{33}$$

where $c_{p,i}^{(g)} = \left(c_{p,H_2}^{(g)}, c_{p,O_2}^{(g)}, c_{p,H_2O}^{(g)}, c_{p,N_2}^{(g)}\right)$ are the specific heat capacities of hydrogen, oxygen, water and nitrogen. The mass diffusion coefficients for each species i depends on the local temperature and pressure, defined as

$$D_i^{(g)}\left(T, p^{(g)}\right) = \left(\frac{T}{T_0}\right)^{3/2} \left(\frac{p_0^{(g)}}{p^{(g)}}\right) D_{i,0}^{(g)}\left(T_0, p_0^{(g)}\right) \tag{34}$$

where $D_{i,0}^{(g)}$ is the diffusion coefficient for each species i at a given temperature T_0 and gas pressure $p_0^{(g)}$. Furthermore, in porous media, we apply the Bruggeman correction and consider pore blockage due to the presence of liquid water (Wang and Wang 2006)

$$D_{i,\text{eff}}^{(g)} = \left(1-s\right) \varepsilon^{3/2} D_i^{(g)} \tag{35}$$

The relative humidity (%) which determines the water content at the anode and cathode inlet is defined as

$$H = \frac{p_{H_2O}^{(g)}}{p_{H_2O}^{\text{sat}}} \times 100 \tag{36}$$

where $p_{H_2O}^{(g)}$ is the partial pressure of water vapour, defined as

$$p_{\text{H}_2\text{O}}^{(g)} = x_{\text{H}_2\text{O}}^{(g)} p^{(g)} \tag{37}$$

and $p_{\text{H}_2\text{O}}^{\text{sat}}$ is the saturation pressure, given by

$$p_{\text{H}_2\text{O}}^{\text{sat}} = p^{\text{ref}} \times 10^{c_1 + c_2(T-T_0) + c_3(T-T_{00})^2 + c_4(T-T_0)^3} \tag{38}$$

The mass fraction of water vapour at the anode and cathode inlet can be determined from

$$\omega_{\text{H2O,a}}^{\text{in}} = \omega_{\text{H2O,c}}^{\text{in}} = \frac{p_{\text{H}_2\text{O}}^{\text{sat}} M_{\text{H}_2\text{O}}\left(\text{H}_{\text{a,c}}^{\text{in}}/100\right)}{p^{(g)} M^{(g)}} \tag{39}$$

By retaining the ratio $x_{\text{O}_2}^{(g)} / x_{\text{N}_2}^{(g)} = 21/79$, the mass fraction of oxygen at the cathode inlet can be calculated from

$$\omega_{\text{O}_2,\text{c}}^{\text{in}} = \frac{M_{\text{O}_2}}{1 + 79/21}\left[\frac{1}{M^{(g)}} - \frac{\omega_{\text{H}_2\text{O,c}}^{\text{in}}}{M_{\text{H}_2\text{O}}}\right] \tag{40}$$

while the mass fraction of hydrogen at the anode inlet is defined as

$$\omega_{\text{H}_2,\text{a}}^{\text{in}} = 1 - \omega_{\text{H}_2\text{O,a}}^{\text{in}} \tag{41}$$

The mass flow inlet in the anode and cathode are defined as

$$\dot{m}_{\text{a}}^{\text{in}} = \xi_{\text{a}}^{\text{in}} \frac{M_{\text{H}_2}}{2F\omega_{\text{H}_2,\text{a}}^{\text{in}}} i_{\text{ave}} A_{\text{cl}} \tag{42}$$

$$\dot{m}_{\text{c}}^{\text{in}} = \xi_{\text{c}}^{\text{in}} \frac{M_{\text{O}_2}}{4F\omega_{\text{O}_2,\text{c}}^{\text{in}}} i_{\text{ave}} A_{\text{cl}} \tag{43}$$

where $\xi_{\text{a,c}}^{\text{in}}$ is the anode and cathode inlet stoichiometry, A_{cl} is the catalyst surface area and i_{ave} is the average current density is given by

$$i_{\text{ave}} = \frac{1}{L}\int_0^L \mathbf{i}^{(s)} \cdot \mathbf{e_y} \, dx \tag{44}$$

where L is the fuel cell length.

The interphase mass transfer for condensation/evaporation of water is defined as (Li 2004)

$$\dot{m}_{\text{H}_2\text{O}} = c_r \max\left((1-s)\frac{p_{\text{H}_2\text{O}}^{(g)} - p_{\text{H}_2\text{O}}^{\text{sat}}}{RT}M_{\text{H}_2\text{O}}, -s\rho^{(l)}\right) \tag{45}$$

where c_r is the condensation/evaporation rate constant. The capillary diffusion for two-phase flow is given by

$$D^{(c)} = \frac{\kappa s^3}{\mu^{(l)}} \frac{dp^{(c)}}{ds}$$ (46)

where the capillary pressure is defined as

$$p^{(c)} = \tau \cos\theta \left(\frac{\varepsilon}{\kappa}\right)^{\frac{1}{2}} J$$ (47)

where τ is the surface tension, θ is the wetting angle, and the Leverett function, J, is defined as

$$J = 1.417(1-s) - 2.12(1-s)^2 + 1.263(1-s)^3$$ (48)

4. Electrochemistry and agglomerate model

We consider an agglomerate model for the electrochemistry at the cathode side and retain a simple Butler-Volmer-type expression for the anode catalyst layer (Sasmito and Mujumdar, 2011)

$$J_a = j_a^{ref} \left(\frac{c_{H_2}^{(g)}}{c_{H_2,ref}^{(g)}}\right)^{1/2} \left[\exp\left(\frac{\alpha_a^{ox}F}{RT}\eta_a\right) - \exp\left(\frac{-\alpha_c^{ox}F}{RT}\eta_a\right)\right]$$ (49)

$$J_c = j_c^{ref} \left(\frac{c_{O_2}^{(g)}}{c_{O_2,ref}^{(g)}}\right) \left[-\exp\left(\frac{\alpha_a^{rd}F}{RT}\eta_c\right) + \exp\left(-\frac{\alpha_c^{rd}F}{RT}\eta_c\right)\right] (1-\gamma_{cl}) \left(1 - \frac{\gamma^{(p)}}{\gamma^{(agg)}}\right) \frac{RT}{H_{O_2}^{(p)}} \xi_1 \frac{1}{1+\xi_2+\xi_3}$$ (50)

The agglomerate model introduces additional mass transfer resistances in the cathode catalyst layer via mass transport inside the spherical agglomerate and the polymer and liquid water films. In Eqs. 47 and 48, $j_{a,c}^{ref}$ and $\alpha_{a,c}^{ox,rd}$ are the volumetric exchange current density and transfer coefficient for anode/cathode oxidation/reduction reaction, respectively. In Eq. 48, $H_{O_2}^{(p)}$ is Henry's constant for the air-ionomer interface, $c_{H_2,ref}^{(g)}$ and $c_{O_2,ref}^{(g)}$ are the reference concentration for hydrogen and oxygen, and ξ_1, ξ_2 and ξ_3 are the correction factors due to resistances of the agglomerate, the polymer and liquid water films, respectively. Furthermore, γ_{cl} represents the volume fraction of pores in the catalyst layer, while $\gamma^{(p)}$ and $\gamma^{(agg)}$ are the volume fraction of polymer and agglomerate, respectively. The cathode volumetric reference exchange current density, j_c^{ref}, is corrected for temperature via Arrhenius-type relation

$$j_c^{ref} = j_{c,0}^{ref} \exp\left[-\frac{E_a}{R}\left(\frac{1}{T} - \frac{1}{T_1}\right)\right]$$ (51)

The overpotentials are defined as

$$\eta_a = \phi^{(s)} - \phi^{(m)} \tag{52}$$

$$\eta_c = \phi^{(s)} - \phi^{(m)} - E_{rev} \tag{53}$$

Where the reversible potential, E_{rev}, is written as

$$E_{rev} = E_{rev,0} - e_1\left(T - T_2\right) + \frac{RT}{4F}\ln x_{O_2}^{(g)} \tag{54}$$

The reference concentration, $c_{i,ref}^{(g)}$, is given by

$$c_{i,ref}^{(g)} = \frac{p^{ref}}{H_i^{(p)}} \tag{55}$$

The correction factor due to the agglomerate is defined as the effectiveness of the mass transfer of oxygen through the spherical agglomerate nucleus, and is given as:

$$\xi_1 = \frac{1}{\Phi}\left(\frac{1}{\tanh(3\Phi)} - \frac{1}{3\Phi}\right) \tag{56}$$

$$\Phi = \frac{r^{(agg)}}{3}\sqrt{\frac{k_c}{D_{O_2,eff}^{(agg)}}} \tag{57}$$

where $r^{(agg)}$ is the agglomerate radius, and k_c is the reaction rate constant, defined as

$$k_c = \frac{j_c^{ref}\left(1 - \frac{\gamma^{(p)}}{\gamma^{(agg)}}\right)\left(-\exp\left(\frac{\alpha_a^{rd}F}{RT}\eta_c\right) + \exp\left(-\frac{\alpha_c^{rd}F}{RT}\eta_c\right)\right)}{4Fc_{O_2}^{ref}} \tag{58}$$

The effective diffusion coefficient of oxygen in polymer inside agglomerate, $D_{O_2,eff}^{(agg)}$, is given by the diffusion coefficient of oxygen in polymer film, $D_{O_2}^{(p)}$, with the Bruggeman correlation

$$D_{O_2,eff}^{(agg)} = D_{O_2}^{(p)}\left(\frac{\gamma^{(p)}}{\gamma^{(agg)}}\right)^{1.5} \tag{59}$$

The correction factor due to polymer film is calculated as

$$\xi_2 = \frac{\delta^{(p)}}{D_{O_2}^{(p)}}\frac{\xi_1}{a^{(p)}}k_c \tag{60}$$

where the polymer film thickness, $\delta^{(p)}$, is defined as

$$\delta^{(p)} = \sqrt[3]{\left(r^{(agg)}\right)^3 \left(1 + \frac{\gamma^{(p)}}{\gamma^{(PtC)}}\right)} - r^{(agg)} \tag{61}$$

and the agglomerate surface area per unit volume of catalyst layer, $a^{(p)}$, is given by

$$a^{(p)} = 4\pi n^{(agg)} (r^{(agg)} + \delta^{(p)})^2 \tag{62}$$

where $n^{(agg)}$ is the number of agglomerates per unit volume, defined as

$$n^{(agg)} = \frac{3\gamma^{(agg)}}{4\pi \left(r^{(agg)} + \delta^{(p)}\right)^3} \tag{63}$$

The correction factor due to liquid water film

$$\xi_3 = \frac{\delta^{(l)}}{D_{O_2}^{(l)}} \frac{\xi_1}{a^{(l)}} k_c \frac{H_{O_2}^{(l)}}{H_{O_2}^{(p)}} \tag{64}$$

where $H_{O_2}^{(l)}$ is Henry's constant for the air-water interface, $D_{O_2}^{(l)}$ is the diffusion coefficient of oxygen in the liquid water , $\delta^{(l)}$ is the thickness of liquid film and $a^{(l)}$ is the surface area of the agglomerate including liquid water per unit volume, defined as

$$\delta^{(l)} = \sqrt[3]{\left(r^{(agg)} + \delta^{(p)}\right)^3 \left(1 + \frac{\gamma^{(l)}}{\gamma^{(agg)}}\right)} - \left(r^{(agg)} + \delta^{(p)}\right) \tag{65}$$

$$a^{(l)} = 4\pi n^{(agg)} (r^{(agg)} + \delta^{(p)} + \delta^{(l)})^2 \tag{66}$$

where the volume fraction of liquid water, $\gamma^{(l)}$, is expressed as function of the liquid saturation, s, by

$$\gamma^{(l)} = \frac{V^{(l)}}{V_{tot}} = s\gamma_{cl} \tag{67}$$

The carbon loading, $L^{(C)}$, and mass fraction of polymer loading in the catalyst layer, $\omega^{(p)}$ are

$$L^{(C)} = \frac{L^{(Pt)}}{\omega^{(Pt)}} - L^{(Pt)} \tag{68}$$

$$\omega^{(p)} = \frac{L^{(p)}}{L^{(Pt)} + L^{(C)} + L^{(p)}} \tag{69}$$

providing the following relationship for the volume fraction of platinum and carbon

$$\gamma^{(\text{PtC})} = \frac{V^{(\text{PtC})}}{V_{\text{tot}}} = \left[\frac{1}{\rho^{(\text{Pt})}} + \frac{1-\omega^{(\text{Pt})}}{\rho^{(\text{C})}\omega^{(\text{Pt})}}\right]\frac{L^{(\text{Pt})}}{h_{\text{cl}}} \tag{70}$$

Here, volume fraction of polymer and agglomerate given by

$$\gamma^{(\text{p})} = \frac{V^{(\text{p})}}{V_{\text{tot}}} = \frac{\omega^{(\text{p})}}{1-\omega^{(\text{p})}}\frac{1}{\rho^{(\text{m})}}\frac{L^{(\text{Pt})}}{\omega^{(\text{Pt})}h_{\text{cl}}} \tag{71}$$

$$\gamma^{(\text{agg})} = \frac{V^{(\text{agg})}}{V_{\text{tot}}} = \gamma^{(\text{p})} + \gamma^{(\text{PtC})} \tag{72}$$

The porosity of the catalyst layer is defined as

$$\gamma_{\text{cl}} = \frac{V_{\text{void}}}{V_{\text{tot}}} = 1 - \gamma^{(\text{agg})} \tag{73}$$

with

$$
\begin{aligned}
&V^{(\text{agg})} = V^{(\text{PtC})} + V^{(\text{p})}, \; V_{\text{void}} = V^{(\text{g})} + V^{(\text{l})} \\
&V_{\text{tot}} = V^{(\text{agg})} + V_{\text{void}} = V^{(\text{PtC})} + V^{(\text{p})} + V^{(\text{l})}
\end{aligned}
\tag{74}
$$

5. Membrane model

For the membrane the activity and water contents per sulfonic group are given by

$$a = \frac{p_{\text{H}_2\text{O}}^{(\text{g})}}{p_{\text{H}_2\text{O}}^{\text{sat}}} + 2s \tag{75}$$

$$\lambda = \begin{cases} 0.043 + 17.81a - 39.85a^2 + 36a^2 & a \leq 1 \\ 14 + 1.4(a-1) & 1 < a \leq 3 \end{cases} \tag{76}$$

The ionic conductivity is defined as

$$\sigma_{\text{eff}}^{(\text{m})} = \beta^{(\text{m})}\sigma^{(\text{m})} \tag{77}$$

where $\sigma^{(\text{m})}$ is defined as

$$\sigma^{(\text{m})} = (0.514\lambda - 0.326)\exp\left[1268\left(\frac{1}{303.15} - \frac{1}{T}\right)\right] \tag{78}$$

The diffusivity of membrane water content per sulfonic group

$$D_{\text{H}_2\text{O,eff}}^{(\text{m})} = \beta^{(\text{m})}D_{\text{H}_2\text{O}}^{(\text{m})} \tag{79}$$

$$D_{H_2O}^{(m)} = \begin{cases} 3.1 \, x \, 10^{-7} \times \lambda \left(\exp(0.28\lambda) - 1 \right) \exp\left[-2436 / T \right] & \text{for } \lambda \leq 3 \\ 4.17 \, x \, 10^{-8} \times \lambda \left(1 + 161 \exp(-\lambda) \right) \exp\left[-2436 / T \right] & \text{for } \lambda > 3 \end{cases} \tag{80}$$

The electro-osmotic drag coefficient is defined as

$$n_d = 2.5 \frac{\lambda}{22} \tag{81}$$

6. Numerical procedure

The model geometry was created using the Gambit pre-processor software. This software can be used to draw the geometry from 1D to 3D and from simple to complex geometry (CAD). Furthermore, it can be used to create mesh either structured or unstructured mesh, with triangular, tetrahedral, hexahedral and polyhedral meshes. Advanced meshing is achieved by applying boundary layer meshing and size function meshing. Labeling boundary condition and defining zone type, either fluid or solid, for further numerical solution are also available.

The mathematical model of the PEM fuel cell was solved with the commercial multi-purpose CFD software FLUENT (Fluent, 2009). The software is based on the finite volume method where the computational domains are divided into a finite number of control volumes (cells) and all variables are stored at the centroid of each cell. Essentially, the software solves for the standard Navier-Stokes equation together with the scalar transport equations. The latter is heavily modified with User Define Scalar (UDS) and User Define Functions (UDFs). The second order upwind is chosen for the discretization. Furthermore, an iterative solver based on the SIMPLE algorithm is employed to solve the pressure velocity coupling. Note that the open-source CFD code can also be utilized to solve the mathematical framework of PEM fuel cell derived here.

The accuracy of numerical solutions is strongly related to mesh density. A grid independence study was undertaken to ensure mesh independent results. In general, a finer mesh can be expected to produce results that are more accurate; however, it comes at the cost of higher memory requirements and longer computing time. In view of this, a grid independence study was performed to obtain an optimum mesh density that gives sufficiently accurate results at acceptable computational cost.

7. Results and discussion

7.1. Validation

When developing and implementing mathematical models to predict the behaviour of a running PEM fuel cell one needs to pay special attention to validation due to the inherent complexity of the coupled physical and chemical phenomena inside the various functional layers of each cell in the stack. As seen in Fig. 2, the iR-corrected and full polarization curves
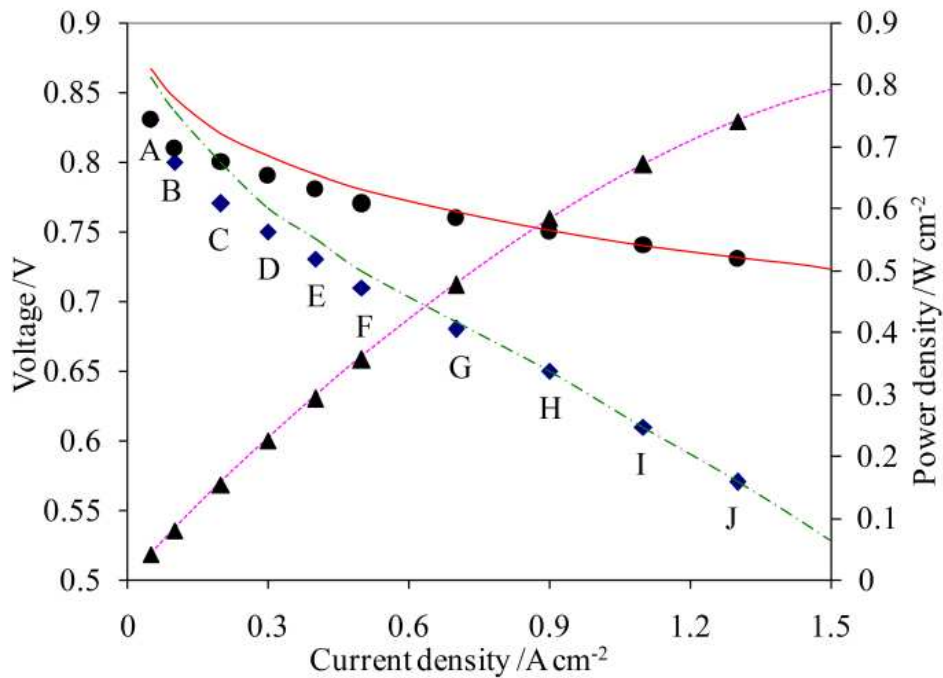
Figure 2. Polarization curves: [♦] is the experimentally measured potential; [●] is the iR-corrected experimentally measured potential; [▲] is the experimentally obtained power density; [– · –] is the predicted potential of the model; [—] is the predicted iR-corrected potential of the model (both case a and b); [- - -] is the predicted power density of the model.
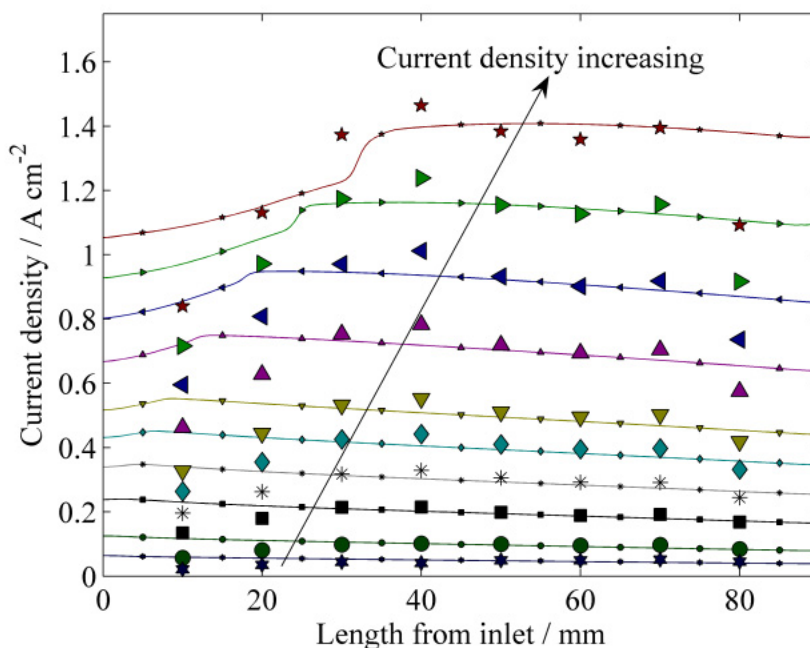

Figure 3. Local current density distribution at the anode terminal in the streamwise direction; symbols correspond to the experimental measurements and lines are model predictions; 1.3 Acm^{-2} (★), 1.1 Acm^{-2} (▶), 0.9 Acm^{-2} (◀), 0.7 Acm^{-2} (▲), 0.5 Acm^{-2} (▼), 0.4 Acm^{-2} (♦), 0.3 Acm^{-2} (✳), 0.2 Acm^{-2} (■), 0.1 Acm^{-2} (●), 0.05 Acm^{-2} (✶).

are in good agreement with experimental data measured by Noponen et al., 2004. Furthermore, the predicted local current density distribution along top of the anode terminal is also compared with its experimental counterpart. For each measured average current density in Fig. 2, denoted by A to J, the local current density distribution was also determined, as depicted in Fig. 3. We see that the model predictions agree well with both iR-corrected and full polarization curves in Fig. 2. We note that at low current densities, the model prediction slightly deviates with maximum relative error of ~ 4% which is good enough for the purposes of this article. Furthermore, the predicted local current density distributions are also in good agreement at lower current densities and start to deviate at the close to the inlet and outlet region at higher current densities. The deviation can most likely be attributed to the placement of the inlet/outlet holes in the experimental setup (see Noponen et al. 2004 for details), which would require a three-dimensional computational domain to resolve properly. This implies that the model correctly account for the fundamental physics associated with PEM fuel cell.

7.2. Thermal management

Thermal management is one of the important keys to efficient operation of PEM fuel cell stacks. In an ideal situation, each fuel cell in the stack would operate under identical operating condition; in reality, however, this is not feasible, as variations inevitably arise due to the design of stack manifold, position of the cell in the stack and choice of thermal management strategy. Efficient and cost-effective cooling of each cell in the stack is necessary to ensure high overall performance. If one removes too much heat, the reaction kinetics are adversely affected and, if water vapor partial pressure exceeds the saturation pressure, water vapor tends to condense which, in turn, lowers stack performance. Conversely, if cooling is not adequate, the stack temperature rises beyond its allowable operating temperature causing the membrane water content and its protonic conductivity to drop, which deteriorates stack performance. It is therefore of interest to understand how various thermal management affect overall stack performance and which strategy to select for a given application.

Broadly speaking, depending on the type of the cathode manifold, the oxygen and/or air flow to the cathode can be supplied directly from ambient air (open cathode) or through a gas manifold. For the former, ambient air is directly supplied to the cathode to provide both the oxidant as well as cooling air. The air flow can be provided by forced convection using a fan, or natural convection due to temperature gradient between the PEM fuel cell stack and the ambient. The former usually can be applied to stack with power rating up to sub kW, while the latter can only be used for small stacks of few cells (depends on the cell geometry) with power rating less than 100 W. For a closed manifold stack, on the other hand, pure oxygen or air is usually supplied by forced convection through a stack manifold and is pre-conditioned, e.g., filtered, heated, and humidified. Therefore, an additional thermal management strategy is usually required. The most common cooling designs include forced convection in specially designed cooling plates/channels with either liquid or air as the coolant, edge cooling with or without fins, and cooling coupled with phase-change materials used for thermal storage.

In practice, the choice of the thermal management strategy depends strongly on details of the specific application and its constraints; for example, in combined heat and fuel cell stationary power systems, liquid cooling (as illustrated in Fig. 1) is preferred since it has larger heat removal rate. Moreover, in this application there is no limitation on the size, weight and complexity of the system as it is used in stationary applications. In small automotive and power generator applications where the weight, size and complexity of the system become the limiting factors, air cooling is preferred due to its simplicity as no coolant loop and heat exchanger are required by the system. An open-cathode PEM fuel cell stack with natural convection cooling has been considered for portable electronic power such as handphone power due to its simplicity.
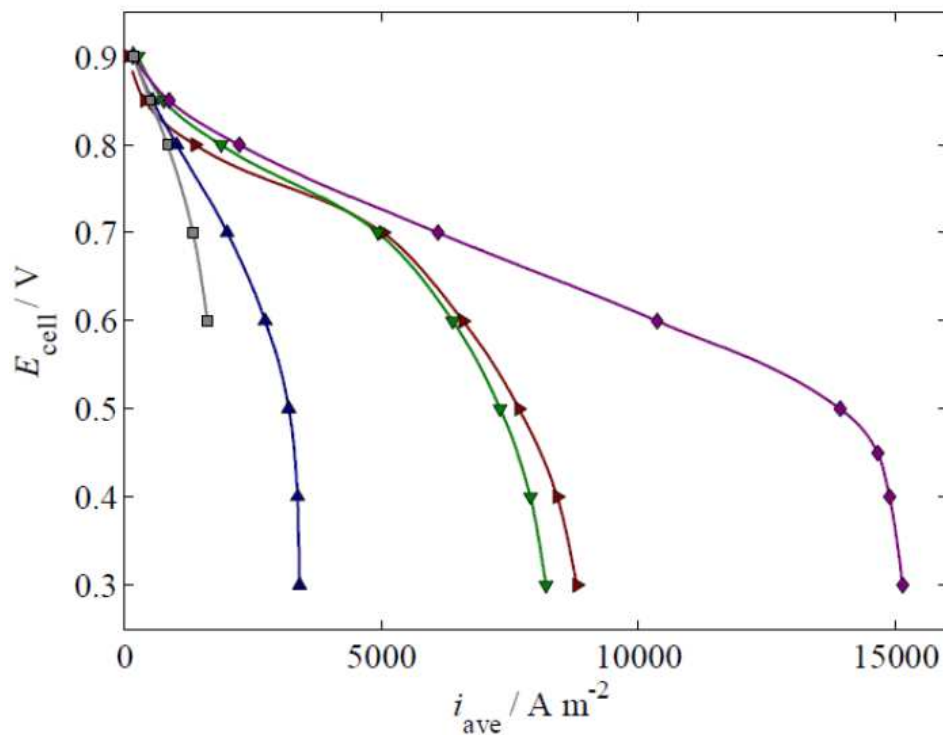

Figure 4. Polarization curves for PEFC stack with liquid cooling (◊); edge cooling (►); air cooling (▼); open-cathode with forced (▲) and natural-air convection (■).

Now, let us have a look at Fig. 4 which displays and compares the predicted stack performance for different thermal management strategies. Here, several features are apparent; foremost is that stack performance is greatly affected by the cooling strategy chosen. It is seen that liquid cooling yields the best results among various alternatives. The natural convection open-cathode stack gives the lowest performance. The computed limiting current density for each case is found to be similar to that found in published experimental investigation: liquid cooling up to 15000 A m⁻² (Noponen et al., 2004), air-cooling up to 8000 A m⁻² (Shimpalee et al., 2009), edge-cooling up to 8500 A m⁻² (Fluckiger et al., 2007), and forced and natural convection with open-cathode up to 3500 A m⁻² (Wu et al., 2009) and 1500 A m⁻² (Urbani et al., 2007), respectively. Conversely, when the complexity, cost, size, weight, and parasitic load are of interest, the order is reversed; for example, stack with

liquid cooling requires a coolant loop, a radiator, a pump, more space and weight as well as additional costs to build the supporting equipment. Natural convection cooling, on the other hand, does not require any additional auxiliary equipment and hence is the least expensive.

7.3. Water management

A PEM fuel cell with a sealed off anode flow field (dead-end anode) has several advantages and also disadvantages. The advantages of this design are that one does not need to consider any excess hydrogen that will exit from the anode outlet if the flow channel is open; presumably all hydrogen is consumed in the fuel cell. However, proper water management is essential in order to keep the membrane sufficiently humidified whilst ensuring that the anode does not flood from water accumulation. In addition, nitrogen can cross over from the cathode side and accumulate at the anode. This can result in a deterioration of cell performance with time as has been reported frequently in the literature.

To avoid operating the anode under adverse conditions, one can purge the accumulated gas-vapor mixture to clear the anode flow field of liquid water and nitrogen. However, this can defeat the main purpose of the dead-end mode as some hydrogen will be lost during the purge and reduce hydrogen utilization. Moreover, it adds complexity to the design as it requires valves and control schemes which result in a parasitic load on the fuel cell. Hence, an optimal or near-optimal purge frequency and duration need to be developed to minimize hydrogen loss, reduce parasitic load, and maintain good fuel cell performance with time.

Starting from purge frequency, two different purge frequencies -- purge every five minutes and every ten minutes -- which is commonly used in a typical PEM fuel cell with a dead-end mode were modelled for 30-second purge duration in each case. With respect to cell performance, it can be expected that purge will recover the cell to its highest performance. This is indeed the case, as seen in Fig. 5, which shows the cell performance drop during dead-end operation and then recovers during purge. It is noted that more frequent purge will keep the cell at a higher performance level compared to that with less frequent ones. In this particular case, a 3 % drop in cell voltage (0.6 V) is observed for the case of more frequent purge (every five minutes), whereas, an 11 % drop (0.55 V) is found for the case of less frequent purge (every 10 minutes) as compared to the open-end case (0.62 V). Further, the performance drop during dead-end operation and performance recovery during purge is mirrored by depletion of the average hydrogen concentration at the anode and its increase during the purge as well as liquid water and nitrogen accumulation and their release (flush-out) during purge (see Fig. 6). More frequent purge results in lower hydrogen depletion, reduced water accumulation, and decreased nitrogen crossover.

Though more frequent purges can maintain higher cell performance, the hydrogen loss is also higher which diminishes the advantage of utilizing a dead-end mode; more parasitic power is also consumed to control the valves, which reduces level of the net power generated. Conversely, if the purge is less frequent, hydrogen utilization is higher which the purpose of dead-end anode mode is. However, the performance can be lower due to greater water and nitrogen accumulation. In addition, purge frequency is also a function of the

volume of anode flow field and gas diffusion layer, flow field type, and operating conditions. Clearly, purge frequency requires careful consideration to ensure a good cell performance whilst maintaining high hydrogen utilization.
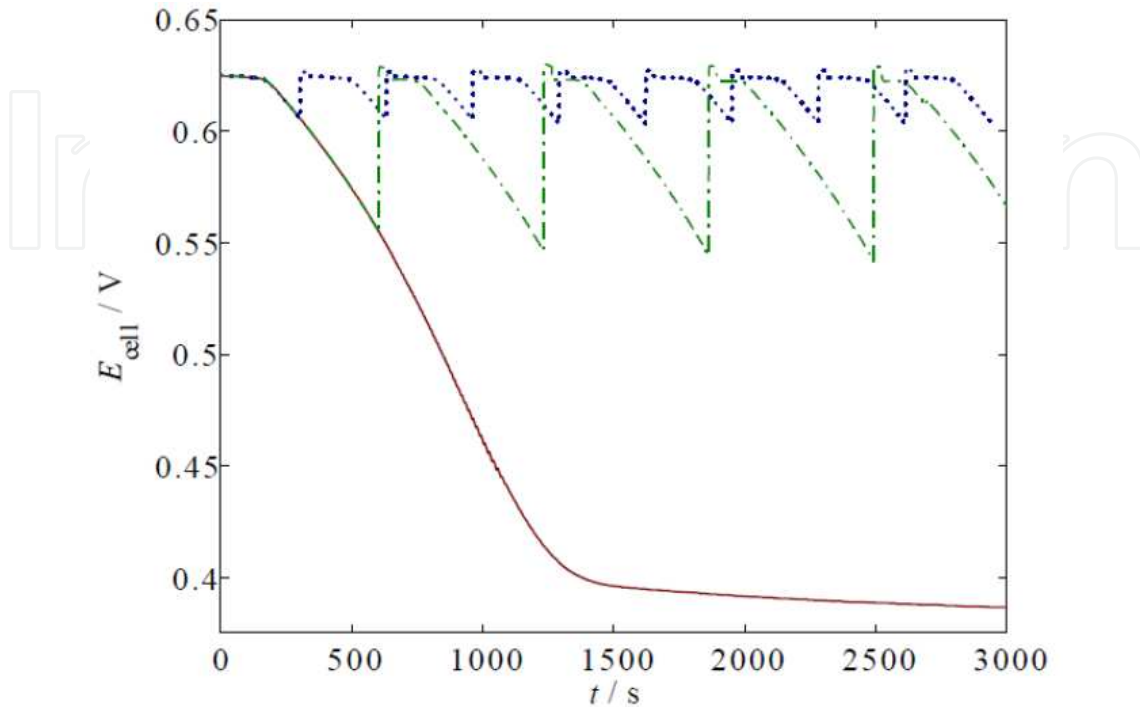

Figure 5. Effect of purge frequency to the cell performance for purging frequency of (···) 5 minutes; (---) 10 minutes; and (—) no purging (base case).

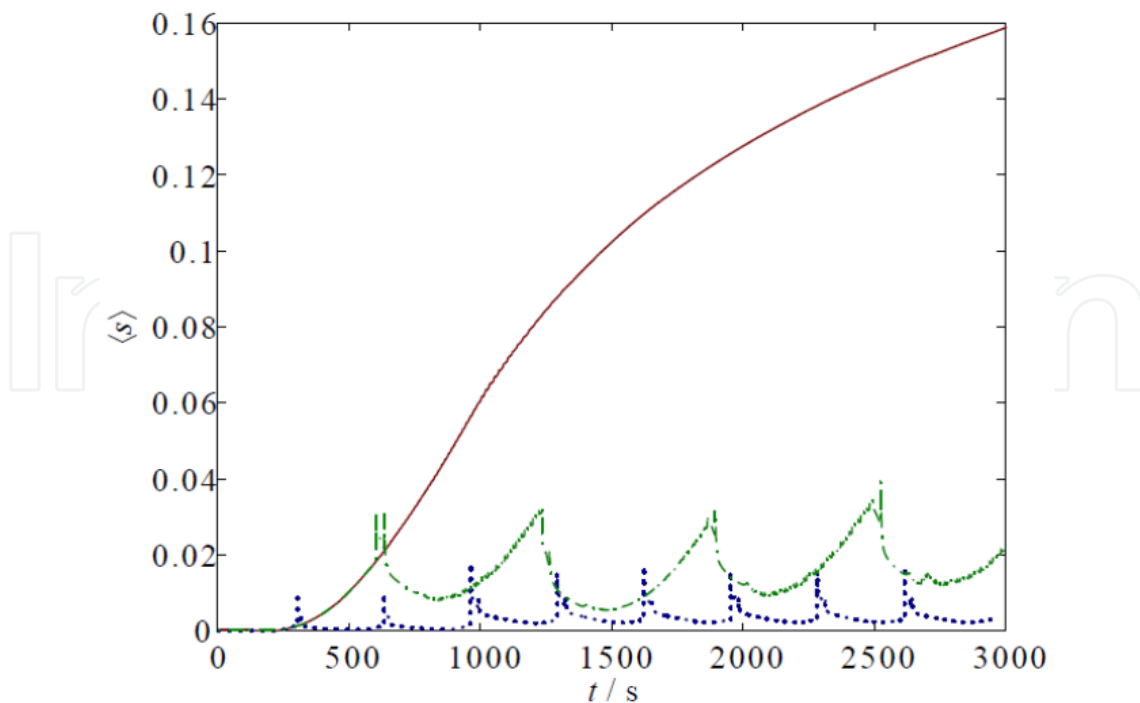**Figure 6.** Effect of purge frequency to the liquid water accumulation for purging frequency of (···) 5 minutes; (---) 10 minutes; and (—) no purging (base case).

7.4. Gas management

Another point of interest in this study is gas management. A good channel design should be able to provide sufficient gas (fuel and oxidant) supply throughout catalyst layer for electrochemical reaction. Here, the oxygen distribution in the cathode catalyst layer is examined. As can be seen in Fig. 7, oxygen concentration is depleted from inlet to outlet as it is consumed for electrochemical reaction. On closer inspection, it reveals that severe oxygen depletion exists at the middle of parallel channel (Fig. 7a). This is attributed to the low velocity and non-uniform oxidant distribution in each passage of the channel, especially at the middle area. Less severe oxygen depletion is observed in the oblique-fin channel, especially at the right-side region (see Fig. 7c for details); this can be due to the presence of secondary flow which leads to flow separation toward outlet region. Serpentine channel, on the other hand, yields the most uniform oxygen distribution and no oxygen depletion is found throughout the cell. This, in combination, indicates that serpentine channel yields the best management among others.
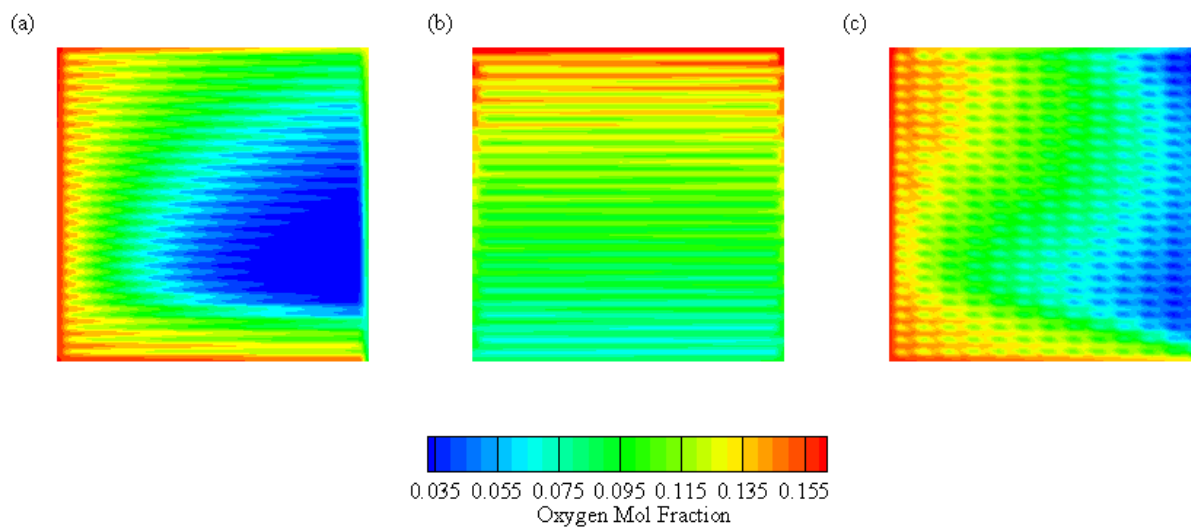

Figure 7. Oxygen mol fraction distribution at cathode catalyst layer for (a) parallel; (b) serpentine; (c) new oblique-fin.

Thus far, the three different channel designs have been evaluated in terms of thermal water and gas management. Now we look further to the fuel cell performance which is represented by current generation in the catalyst layer shown in Fig. 8. Clearly, a good thermal, water and gas management in serpentine channel is mirrored by high stack performance with uniformly distributed current generation (Fig. 8b). In contrast, the oxygen depletion, liquid accumulation and "hot-spot" temperature in parallel channel results in non-uniform and low current generation (~26% lower than serpentine channel). Closer inspection reveals that almost no current is generated in the region where oxygen depletion and liquid accumulation exist. The performance of oblique-fin channel lies in between serpentine and parallel channel: the current density is around 10% lower than serpentine channel and around 16% higher with the degree of uniformity improves up to around 34 % than parallel channel.
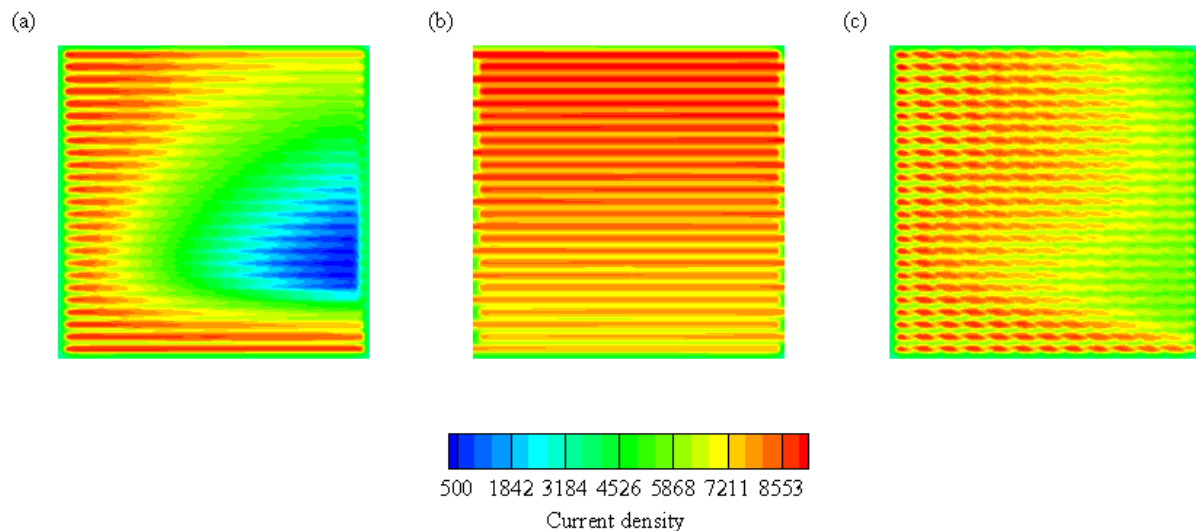
Figure 8. Current density distribution at cathode catalyst layer for (a) parallel, i_{ave} = 6200 A/m²; (b) serpentine, i_{ave} = 8400 A/m²; (c) new oblique-fin channel, i_{ave} = 7400 A/m².

8. Concluding remarks

A computational study was carried out of the transport phenomena in PEM fuel cell for a single cell as well as a stack of fuel cells. The model has good agreement with experimental data for global and iR-corrected curves as well as local current density distribution. Several thermal management strategies, e.g., liquid-cooled, air-cooled, edge-cooled and open-cathode fuel cell with forced and natural convection cooling, were evaluated. It is found that liquid-cooled fuel cell yields the best performance among others; however, it requires the most complex auxiliary system, size and weight.

A transient performance of PEM fuel cell with a dead-end anode was simulated. It is noted purge can maintain fuel cell at high performance as it flush-out accumulated liquid water and other gases which, in turn, recovers hydrogen concentration in the anode side.

Furthermore, three different gas and gas channel designs, e.g., parallel, serpentine and oblique-fin channels were investigated via mathematical model. The serpentine design gives the most uniform oxygen distribution throughout the catalyst layer which is mirrored by high cell performance.

Finally, we note that mathematical modeling plays significant contribution to speed-up the commercialization of the fuel cell as it can assist experimental on addressing main issues in fuel cell research and development, e.g., thermal, gas and water management.

Author details

Agus P. Sasmito, Erik Birgersson and Arun S. Mujumdar
Minerals Metals Materials Technology Centre (M3TC), National University of Singapore, Singapore

Agus P. Sasmito
Mechanical Engineering, Masdar Institute of Science and Technology, Abu Dhabi, United Arab Emirates

Erik Birgersson
Department of Chemical and Biomolecular Engineering, National University of Singapore, Singapore

Arun S. Mujumdar
Mechanical Engineering Department, National University of Singapore, Singapore

Nomenclature

a	Water activity
$a^{(l)}$	Surface are of the agglomerates including water per unit volume, m^{-1}
$a^{(p)}$	Surface area of the agglomerates per unit volume of catalyst layer, m^{-1}
A_{cl}	Catalyst area, m^2
$c_i^{(g)}$	Molar concentration of species i, mol m^{-3}
$c_{i,ref}^{(g)}$	Reference molar concentration of species i, mol m^{-3}
$c_p^{(g)}$	Specific heat capacity of gas mixture, J kg^{-1} K^{-1}
$c_{p,i}^{(g)}$	Specific heat capacity of species i, J kg^{-1} K^{-1}
c_r	Condensation/evaporation rate constant, s^{-1}
c_1, c_2, c_3, c_4	Constants for the saturation pressure of water; -, K^{-1}, K^{-2}, K^{-3}
$D^{(c)}$	Capillary diffusion, m^2 s^{-1}
$D_i^{(g)}$, $D_{i,eff}^{(g)}$	Diffusivity and effective diffusivity of species i, m^2 s^{-1}
$D_{H_2O}^{(m)}$, $D_{H_2O,eff}^{(m)}$	Diffusivity and effective diffusivity of water in the membrane, m^2 s^{-1}
$D_{O_2,eff}^{(agg)}$	Effective diffusion coefficient of oxygen in the agglomerate, m^2 s^{-1}
$D_{O_2}^{(l)}$, $D_{O_2}^{(p)}$	Diffusion coefficient of oxygen in liquid water and in polymer film, m^2 s^{-1}
$\mathbf{e}_x$, $\mathbf{e}_y$, $\mathbf{e}_z$	Coordinate vectors
E_{cell}, E_{stack}	Cell and stack voltage, V
E_a	Activation energy, J mol^{-1}
E_{rev}	Reversible cell potential, V
F	Faraday constant, C mol^{-1}
h_j	Height of layer j, m
$H_{O_2}^{(l)}$, $H_{O_2}^{(p)}$	Henry's constant for air-water and air-polymer interfaces, Pa m^3 mol^{-1}
H_{vap}	Heat of vaporization, J kg^{-1}
H	Relative humidity, %
i, $\mathbf{i}$	Current density, A m^{-2}
$j_{a,c}^{ref}$	Anode and cathode volumetric reference exchange current density, A m^{-3}
J	Volumetric current density, A m^{-3}
J	Leverett function
k	Thermal conductivity, W m^{-1} K^{-1}
k_c	Reaction rate constant, s^{-1}
L	Length of channel, m
$L^{(C)}$, $L^{(p)}$, $L^{(Pt)}$	Carbon, polymer and platinum loading, kg m^{-3}

$\dot{m}_{H_2O}$ Interphase mass transfer due to condensation/evaporation of water, kg m^{-3} s^{-1}

$M^{(g)}$ Mean molecular mass of the gas phase, kg mol^{-1}

M_i Molecular mass of species i, kg mol^{-1}

$M^{(m)}$ Equivalent weight of the dry membrane, kg mol^{-1}

$n^{(agg)}$ Number of agglomerates per unit volume, m^{-3}

n_d Electroosmotic drag coefficient

$\mathbf{n}_i^{(g)}$, $\mathbf{n}_{H_2O}^{(m)}$ Mass flux of species i and water in the membrane, kg m^{-2} s^{-1}

$P^{(c)}$, $p^{(g)}$ Capillary and gas pressure, Pa

$p_{H_2O}^{sat}$ Saturation pressure of water, Pa

R Gas constant, J mol^{-1} K^{-1}

$r^{(agg)}$ Radius of agglomerate, m

Re Reynolds number

s Liquid saturation

S Source term

T_0, T_1, T_2 Constant, K

T Temperature, K

$\mathbf{u}$, u, v, U Velocities, m s^{-1}

V Volume, m^3

$x_i^{(g)}$ Molar fraction of species i

x, y, z Coordinates, m

$\omega_i^{(g)}$ Mass fraction of species i

$\omega^{(p)}$ Mass fraction of polymer loading

$\omega^{(Pt)}$ Mass fraction of platinum loading on carbon

Greek

α Transfer coefficient

$\beta^{(m)}$ Membrane modification coefficient

γ Volume fraction

δ Thickness of the film, m

ε Porosity

η Overpotential, V

θ Wetting angle

κ Permeability, m^2

λ Membrane water content

μ Dynamic viscosity, kg m^{-1} s^{-1}

ξ Stoichiometry

ξ_1, ξ_2, ξ_3 Correction factors for agglomerate model

ρ Density, kg m^{-3}

τ Surface tension, Pa

σ Total stress tensor, Pa

σ Conductivity S m^{-1}

ϕ Potential, V

$\Phi_{\alpha,\beta}$ Dimensionless quantities

Φ   Thiele modulus

Superscripts

(agg)   Agglomerate
(c)   Capillary
(C)   Carbon
cool   Coolant
(g)   Gas phase
in   Inlet
(l)   Liquid phase
(m)   Membrane
ox   Oxidation
(p)   Polymer phase
(Pt)   Platinum
(PtC)   Platinum and carbon
rd   Reduction
ref   Reference
(s)   Solid
sat   Saturation
set   Setting

Subscripts

α, β Index for species
a   Anode
ave   Average
c   Cathode
cc   Current collector
cl   Catalyst layer
co   Coolant channel
eff   Effective
cool   Coolant
eff   Effective
ff   Flowfield
gdl   Gas diffusion layer
H_2 Hydrogen
H_2O Water
i   Species i
iR   iR-corrected
j   Functional layer j
m   Membrane
mass   Mass
N_2 Nitrogen
O_2 Oxygen

pot   Potential
ref   Reference
sp   Separator plate
temp   Temperature
tot   Total
void   Void
0   Standard conditions

9. References

Brujin, F. A. de; Dam, V. A. T.; Janssen, G. J. M. Review: Durability and degradation issues of PEM fuel cell components, Fuel Cells 8 (2007) 3-22.

Costamagna, P.; Srinivasan, S. Quantum jump in the proton exchange membrane fuel cell science and technology from 1960 to the year 2000, part 1: Fundamental scientific aspect, J. Power Sources 102 (2001a) 242-252.

Costamagna, P.; Srinivasan, S. Quantum jump in the proton exchange membrane fuel cell science and technology from 1960 to the year 2000, part 2: Engineering, technology development and applications aspect, J. Power Sources 102 (2001b) 253-269.

Fluckiger, R.; Tiefenauer, A.; Ruge, M.; Aebi, C.; Wokaun, A.; Buchi, F. N. Thermal analysis and optimization of a portable edge-air-cooled PEFC stack, J. Power Sources 172 (2007) 324-333.

FLUENT PEMFC module, http://www.fluent.com, accessed 2009.

Hellman, H. L.; Hoed, R. V. D. Characterizing fuel cell technology challenge of the commercialization process, Int. J. Hydrogen Energy 32 (2007) 305-315.

Hermann, A.; Chaudhuri, T.; Spagnol, P. Bipolar plates for PEM fuel cells: A review, Int. J. Hydrogen Energy 30 (2005) 1297-1302.

Li, S. and Becker, U., A Three Dimensional Model for PEMFC, ASME Proc. 2nd Fuel Cell Science Engineering and Technology, Rochester, New York 2 (2004) 157-164.

Noponen, M., Birgersson, E., Ihonen, J., Vynnycky, M., Lundblad, A., Lindbergh, G., A Two-phase Non-isothermal PEFC, Model: theory and validation, Fuel Cells, 4 (2004) 365-377.

Martin, K. E.; Kopasz, J. P.; McMurphy, K. W. Status of fuel cells and the challenges facing fuel cell technology today, American Chemical Society, 2010.

Mock, P.; Schmid, S. A. Fuel cells for automotive power trains: A techno-economic assessment, J. Power Sources 190 (2009) 133-140.

Sasmito, A.P.; Mujumdar, A.S. Transport phenomena models for polymer electrolyte fuel cell stacks: thermal, water and gas management – From fundamental to application, *Lambert Academic Publishing,* Germany 2011. ISBN: 978-3-8443-9063-6.

Sasmito, A.P.; Birgersson, E.; Mujumdar, A.S. Numerical Evaluation of Various Thermal Management Strategies for Polymer Electrolyte Fuel Cell Stacks, International Journal of Hydrogen Energy 36 (2011a) 12991-13007.

Sasmito, A.P.; Lum, K.W.; Birgersson, E.; Mujumdar, A.S. Computational study of forced air-convection in open-cathode polymer electrolyte fuel cells stacks, Journal of Power Sources 195 (2010) 5550-5563.

Sasmito, A.P.; Birgersson, E.; Lum, K.W.; Mujumdar, A.S. Fan selection and stack design for open-cathode polymer electrolyte fuel cell stacks, Renewable Energy 37 (2012b) 325-332.

Sasmito, A.P.; Birgersson, E.; Mujumdar, A.S. Numerical investigation of liquid water cooling for a proton exchange membrane fuel cell stack, Heat Transfer Engineering 32 (2011c) 151-167.

Sasmito, A.P.; Mujumdar, A.S.; Performance Evaluation of a Polymer Electrolyte Fuel Cell with a Dead-End Anode: A Computational Fluid Dynamic Study, International Journal of Hydrogen Energy 36 (2011d) 10917-10933.

Sasmito, A.P.; Kurnia, J.C.; Birgersson, E.; Mujumdar, A.S. Numerical Evaluation of Performance of Oblique-Fin Channel for PEM Fuel Cell Stacks Relatives to Conventional Channels, 3rd International Conference on Fuel Cell and Hydrogen Technology 2011, Kuala Lumpur, Malaysia, 2011e.

Schwarz, D. H.; Djilali, N., 3D Modeling of Catalyst Layer in PEM Fuel Cells Effect of Transport Limitation, J. Electrochem. Soc., 154 (2007) B1167 - B1178.

Shimpalee, S.; Ohashi, M.; Zee, J. W. V.; Ziegler, C.; Stoeckmann, C.; Sadeler, C.; Hebling, C. Experimental and numerical studies of portable PEMFC stack, Electrochim. Acta 54 (2009) 2899-2911.

Staffell, I.; Green, R. J. Estimating future prices for stationary fuel cells with empirically derived experienced curves, Int. J. Hydrogen Energy 34 (2009) 5617-5628.

Steiner, N. Y.; Mocoteguy, P.; Candusso, D.; Hissel, D. A review on polymer electrolyte membrane fuel cell catalyst degradation and starvation issues: causes, consequences and diagnostic for mitigation, J. Power Sources 194 (2009) 130-145.

Sopian, K.; Daud, W. R. W. Challenges and future developments in proton exchange membrane fuel cells, Renewable Energy 31 (2006) 719-727.

Tsuchiya, H.; Kobayashi, O. Mass production cost of PEM fuel cells by learning curve, Int. J. Hydrogen energy 29 (2004) 985-990.

Urbani, F.; Squadrito, G.; Barbera, O.; Giacoppo, G.; Passalacqua, E.; Zerbinati, O. Polymer electrolyte fuel cell mini power unit for portable application, Journal of Power Sources 169 (2) (2007) 334-337.

Wang, Y. and Wang, C.Y., A Non-isothermal, Two-phase Model for Polymer Electrolyte Fuel Cells, J. Electrochem. Soc., 153 (2006) A1193-A12000.

Wee, J. H. Applications of proton exchange membrane fuel cell systems, Renewable Sustainable Energy Rev. 11 (2007) 1720-1738.

Wu, J.; Galli, S.; Lagana, I.; Pozio, A.; Monetelone, G.; Yuan, X. Z. An air-cooled proton exchange membrane fuel cell with combined oxidant and coolant flow, J. Power Sources 188 (2009) 199-204.